Cholesterol-laden brain-permeable nanoparticles support long-lasting cognitive recovery and motor amelioration in the slow-progressing zQ175DN mouse model of Huntington's Disease

Giulia Birolini[†1,2], Marta Valenza[†§1,2], Ilaria Ottonelli[3], Francesca Talpo[4], Lucia Minoli[5,7], Andrea Cappelleri[6,7], Mauro Bombaci[2], Claudio Caccia[8], Valerio Leoni[9], Alice Passoni[10], Monica Favagrossa[10], Maria Rosaria Nucera[1,2], Laura Colombo[10], Saverio Paltrinieri[11], Renzo Bagnati[10], Jason Thomas Duskey[3], Riccardo Caraffi[3], Maria Angela Vandelli[3], Franco Taroni[8], Mario Salmona[10], Eugenio Scanziani[6,7], Gerardo Biella[4], Barbara Ruozi[3], Giovanni Tosi[3], Elena Cattaneo[1,2§]

[†]**These authors contributed equally to this work**

[§]**Co-corresponding authors**

Abstract

Huntington's disease (HD) has been linked to reduced synthesis of cholesterol in the brain. Its exogenous delivery to the brain has been shown to be beneficial in the rapidly progressing R6/2 mouse model. Here we used an advanced formulation of brain-permeable nanoparticles (NPs) loaded with cholesterol and called hybrid-g7-NPs-chol, to explore the long-term therapeutical potential of cholesterol administration to the brain of the slow-progressing zQ175DN knock-in HD mouse model.

We show that one cycle treatment with hybrid-g7-NPs-chol, administered in the pre-symptomatic or symptomatic phases, is sufficient to completely normalize cognitive defects up to 5 months, as well as to improve other behavioral and neuropathological parameters. Instead, two cycles of hybrid-g7-NPs-chol are needed to achieve long-lasting therapeutic benefits for 12 months without severe inflammatory side-effects. Sustained cholesterol delivery to the brain

of zQ175DN mice also reduces mutant Huntingtin aggregates both in striatum and cortex and completely normalizes glutamatergic communication in the striatal medium spiny neurons compared to saline-treated HD mice.

These results show that cholesterol delivery via brain-permeable NPs is a safe and versatile therapeutic option for lastingly reversing HD-related behavioral decline and neuropathological signs, highlighting the translational potential of cholesterol-based strategies in HD patients.

Author affiliations:

1. Department of Biosciences, University of Milan, 20133 Milan, Italy

2. Istituto Nazionale di Genetica Molecolare "Romeo ed Enrica Invernizzi", 20122 Milan, Italy

3. Nanotech Lab, Te.Far.T.I. Center, Department of Life Sciences, University of Modena and Reggio Emilia, 41125 Modena, Italy

4. Department of Biology and Biotechnologies, University of Pavia, 27100 Pavia, Italy

5. Dipartimento di Scienze Veterinarie, Università degli Studi di Torino, 10095 Grugliasco, Italy

6. Dipartimento di Medicina Veterinaria e Scienze Animali, Università degli Studi di Milano, 26900 Lodi, Italy

7. Mouse & Animal Pathology Lab (MAPLab), Fondazione UniMi, 20139 Milan, Italy

8. Unit of Medical Genetics and Neurogenetics. Fondazione IRCCS Istituto Neurologico Carlo Besta, 20131 Milan, Italy.

9. Laboratory of Clinical Chemistry, Hospital Pio XI of Desio, ASST-Brianza and Department of Medicine and Surgery, University of Milano Bicocca, 20900 Monza, Italy.

10. Istituto di Ricerche Farmacologiche Mario Negri IRCCS, 20156 Milan, Italy

11. Dipartimento di Medicina Veterinaria e Scienze Animali, Università degli Studi di Milano, 26900 Lodi, Italy

Correspondence to:

Elena Cattaneo and Marta Valenza

Department of Biosciences, University of Milan, 20133 Milan, Italy

Istituto Nazionale di Genetica Molecolare "Romeo ed Enrica Invernizzi", 20122 Milan, Italy

elena.cattaneo@unimi.it

marta.valenza@unimi.it

Running title: Cholesterol promotes lasting recovery in HD

Keywords: Cholesterol; Huntington's disease; brain delivery; nanoparticles; cognitive decline

Abbreviations: 24S-OHC = 24S-hydroxycholesterol; AC = activity cage test; APCI = atmospheric pressure chemical ionization; BBB = blood-brain barrier; BHT = butylated hydroxytoluene; Cm = membrane capacitance; Cyp46a1 = cholesterol 24-hydroxylase; CS = conditioned stimulus; FC = fear conditioning test; GC–MS = gas chromatography - mass spectrometry; G-CSF = granulocyte colony-stimulating factor; GM-CSF = granulocyte/macrophage colony-stimulating factor; GS = grip strength test; HD = Huntington's disease; HTT = Huntingtin; ID-GC-MS = isotope dilution-gas chromatography-mass spectrometry; IP = intraperitoneal injection; LC-MS = Liquid chromatography-mass spectrometry; mEPSCs = miniature excitatory post- synaptic currents; MIP-1a and MIP-1b = macrophage inflammatory protein; MSNs = medium- sized spiny neurons; MRM = multiple reaction monitoring; NOR = novel object recognition test; NPs = nanoparticles; PC = paw clasping test; PCA = principal component analysis; PDI = polydispersity index; PLGA = poly-lactic-co-glycolic acid; Rin = input resistance; RR = Rotarod test; SEM = standard error of the mean; sEPSCs = spontaneous excitatory post-synaptic currents; SREBP2 = Sterol regulatory element-binding protein 2; TTX = Tetrodotoxin; wt = wild-type; UC = unconditioned stimulus; YM = Y-maze test.

Introduction

An increasing number of studies highlight the importance of cholesterol homeostasis for brain function. Disruption of cholesterol synthesis and/or catabolism in the brain is associated with several neurological disorders, including Huntington's disease (HD), an autosomal dominant neurodegenerative disease with adult-onset, caused by the expansion of a polyglutamine-encoding cytosine adenine guanine (CAG) tract in exon 1 of the huntingtin (HTT) gene[1]. Due to this mutation, the striatal medium spiny neurons (MSNs) and cortical neurons projecting to the striatum progressively degenerate, causing motor defects, cognitive decline, and psychiatric disturbance[2,3].

Among the underlying pathogenetic mechanisms, twenty years of experimental activity demonstrated a significant reduction in the cholesterol biosynthesis in the HD brain of rodents, with early and massive involvement of the striatum[4-6]. Reduced level of the cholesterol precursors lanosterol, desmosterol and lathosterol measured by isotope dilution-gas chromatography-mass spectrometry (ID-GC-MS) was found in brain samples collected from different rodent models of HD from pre-symptomatic stages[4,5,7]. This finding was mirrored by evidence of a reduced rate of *de novo* cholesterol biosynthesis in the striatum of knock-in HD mouse model[7]. 24-S-hydroxycholesterol (24S-OHC) is the brain-specific cholesterol catabolite which, unlike cholesterol, crosses the blood-brain barrier (BBB) and can be detected in plasma. The reduced level of 24S-OHC measured in plasma from HD patients is consistent with a defect in cholesterol biosynthesis in brain, although it may also reflect ongoing neuronal loss[8-10]. Since peripheral cholesterol is unable to cross the BBB[11] and local synthesis of cholesterol is critical for neuronal function and synaptic transmission[12,13], its reduced biosynthesis can contribute to the severe cognitive and synaptic defects observed in the disease, as well as other dysfunctions[2,3].

The abovementioned results led to investigate the effect of exogenous cholesterol administration in the HD brain. This was first studied in R6/2 mice, an HD mouse line showing early and rapid progression of behavioural, molecular, and electrophysiological disease signatures, starting at 6 weeks of age. As a carrier of exogenous cholesterol, brain-permeable polymeric nanoparticles (NPs) made-up of poly-lactic-co-glycolic acid (PLGA), modified on their surface with the endogenous g7 shuttle-peptide for brain penetration and loaded with cholesterol, called g7-PLGA-NPs-chol, were used to allow cholesterol to pass through the BBB after intraperitoneal (ip) injection. With this strategy, the amount of cholesterol delivered was

estimated to be around 15 µg and sufficient to prevent cognitive decline and improve synaptic dysfunction in R6/2 mice. However, motor behavior was not significantly affected[14].

Subsequent dose-dependent studies performed in the same R6/2 mice using osmotic minipumps allowed to infuse three increasing doses of cholesterol directly into the striatum in a constant and continuous way. The maximum dose of 369 µg of cholesterol infused in 4 weeks was identified as the dose able to restore both cognitive and motor abnormalities, to normalize synaptic morphology and transmission defects, and to counteract the aggregation of mutant HTT (muHTT)[15]. Consistent with the data cited above[14], the low and medium infused doses of 15 and 185 µg were also equally able to prevent cognitive decline, however they did not produce any effect on motor performance, suggesting that full recovery depends on the dose of cholesterol administered and that a low amount of cholesterol is sufficient to normalize cognition, but a high dose is necessary for motor recovery.

More recently, an advanced formulation of NPs has been developed that efficiently combines g7-PLGA and cholesterol to improve their structural characteristics and carrying capacity of the cholesterol moiety. These NPs, named hybrid-g7-NPs-chol, carried about 30-times more cholesterol than g7-PLGA-NPs-chol[16] and led to a partial rescue of motor benefits in R6/2 mice[17]. However, the slow release of cholesterol from hybrid-g7-NPs-chol (several weeks) combined with the rapid progression of R6/2 mice (survival time of 13 weeks) did not allow to fully exploit the benefits of the treatment[17].

Here, we addressed the question of the long-term potential of hybrid-g7-NPs-chol to modify disease progression in the slow-progressing heterozygous (het) zQ175DN (delta neo) knock-in mouse model. This mouse model closely mimics the human mutation since the neo-deleted knock-in allele encoding the human HTT exon 1 sequence with a ~190 CAG repeat tract is inserted into the mouse huntingtin (htt) gene. The data available so far on the progression of the disease in zQ175DN mice (backcrossed to FVB/N, a strain highly susceptible to neurodegeneration) showed a prolonged pre-symptomatic and prodromal phase with the first molecular alterations starting from 3 months of age, cognitive and motor deficits respectively from 6 and 9 months of age, clinical signs, and survival deficits from 12 months of age[18]. Here we exploited these hallmarks to explore the long-term benefits of the hybrid-g7-NPs-chol as the prolonged survival of the animals ensured the complete release of cholesterol from the NPs. The study tested the performance of zQ175DN mice in a C57BL6 background (the mouse line used to maintain the colony) in three different trials: in one trial the animals were treated in a

pre-symptomatic stage; a second trial tested the effectiveness of a late treatment started when symptoms were evident; the third trial mimicked a chronic administration consisting of 2 treatment courses, one early and the other late. Each treatment consisted of 10 injections with hybrid-g7-NPs-chol over a period of 4 weeks (2 injections/week). Long-term improvement in disease phenotypes together with the likelihood of side effects were analyzed. In all studies, the administration of cholesterol to the rodent brain led to full recovery from the cognitive decline associated with disease progression, an effect that was long-lasting and occurred also when treatment was given symptomatically. Reversal of motor defects and massive reduction of muHTT aggregates coincided with the timing of maximum cholesterol release We conclude that cognitive decline in HD rodents is fully treatable for at least 40 consecutive weeks and that cholesterol delivery to the brain is a safe and versatile therapeutic option for HD that can also prevent or counter multiple disease phenotypes.

Materials and methods

NPs production and characterization

Hybrid-g7-NPs loaded with bodipy-chol and labelled with Cy5 (Cy5-hybrid-g7-NPs-bodipy-chol), hybrid-g7-NPs loaded with d6-chol (hybrid-g7-NPs-d6-chol) and hybrid-g7-NPs-chol were prepared and characterized as previously described[16,17]. Briefly, all NPs were produced via a nanoprecipitation method by dissolving 25 mg of polymer and 25 mg of lipid in acetone and using a 0.5% w/V Pluronic® F68 water solution at 45°C as aqueous phase. For each batch, standard nanotechnological characterization was performed to assess NPs quality. Size (nm), polydispersity index (PDI; a value to estimate the uniformity in size of the NPs) and z-potential (mV; a measure reflecting the surface charge of the NPs) were measured with Photon Correlation Spectroscopy (Malvern Zetasizer ZS, Malvern, UK) at a concentration of 0.01 mg/mL (automatic laser attenuator, refractive index 1.59). The mean (± SD) values of these features of all NPs used in this study are herein summarized: size (nm): 249±38; PDI: 0.29±0.05; z-potential (mV): -30±7. The content of cholesterol in each batch was quantified via RP-HPLC-UV (Jasco, Cremella, Italy) using a system equipped with a Syncronis C18 column (250 × 4.6 mm; porosity 5 µm; Thermo Fisher Scientific, Waltham, MA, USA), performing a isocratic separation with 50:50 Acetonitrile:Ethanol as mobile phase (flow rate 1.2 mL/min, UV detector set at 210 nm). Cholesterol was extracted from lyophilized NPs before injection and PLGA was removed. The mean (±SD) cholesterol content was

28.71±3.498 mg of cholesterol for 100 mg of NPs. Data presented were calculated as mean of at least three independent measurements.

zQ175DN colony management and treatment

zQ175DN mice were acquired by The Jackson Laboratories (B6.129S1-*Htt*$^{tm1.1Mfc}$/190ChdiJ; Jax stock #029928; RRID:IMSR JAK:029928). zQ175DN mice colony was maintained using both male and female heterozygous mice by mating 6-weeks old zQ175DN mice with C57BL6/J mice (purchased from Charles River). Mice were weaned and then genotyped at 3 weeks of age (+/- 3 days). Mice were housed under standard conditions in enriched cage (22 ± 1°C, 60% relative humidity, 12 hours light/dark schedule, 3–4 mice/cage, with food and water ad libitum). After PCR genotyping, male and female mice were included and randomly divided into experimental groups. Littermates were included as controls.

All animal experiments were approved and carried out in accordance with Italian Governing Law (D.lgs 26/2014; Authorization n.581/2019-PR issued July 29, 2019 by Ministry of Health and Authorization n.714/2020-PR issued July 21, 2020 by Ministry of Health and); the NIH Guide for the Care and Use of Laboratory Animals (2011 edition) and EU directives and guidelines (EEC Council Directive 2010/63/UE).

7-weeks-old wild-type (wt) littermate mice (for cholesterol release and d6-chol quantification studies) and zQ175DN mice (for the behavioral experiments) were treated with 0.12 mg NPs/gr body weight (about 1.7 mg NPs/mouse; carrying about 493 µg of cholesterol) for ip injection. As controls, wt and zQ175DN littermates were treated with saline solution. For all trials, mice were assigned randomly, and sex was balanced in the various experimental groups; animals from the same litter were divided in different experimental groups; blinding of the investigator was applied to in vivo procedures and all data collection.

Bodipy analysis

Analysis was performed as described in (17). Briefly, 24h, 2 weeks, 10 weeks or 20 weeks after a single ip injection of Cy5-hybrid-g7-NPs-bodipy-chol, mice were deeply anesthetized by ip injection of Avertin 2.5% and transcardially perfused with PFA 4%. Brains were post-fixed for 2h in the same solution at 4°C (not longer to avoid fluorescence bleaching) and then in sucrose

30% to prevent ice crystal damage during freezing in OCT. 15 µm-thick brain coronal sections were counterstained with the nuclear dye Hoechst 33258 (1:10.000, Invitrogen) and then mounted under cover slips using Vectashield mounting medium (Vector Laboratories). The fluorescence signals of Cy5 and bodipy-chol were acquired the following day. To quantify the released bodipy-chol from hybrid-g7-NPs-chol, Volocity software was used using the plug-in "find objects" and "calculate object correlation" (n=4 mice/time point; n=6 images/mouse).

Liquid chromatography-mass spectrometry (LC-MS) analysis for d6-chol quantification

The previously published validated method by Passoni et al. was used[19]. Briefly, an aliquot of plasma (50 µL) was diluted with 200 µL of ethanol containing 200 ng of beta-sitosterol, used as internal standard. Samples were vortexed and centrifuged at 13200 rpm for 15 min and 2 µL of the supernatants were directly injected into the LC-MS system. Each brain area and peripheral tissues were homogenized in 1 mL of PBS, containing 500 ng of internal standard. 200 µL of homogenate were extracted with 800 µL of ethanol, vortexed, and centrifuged for 15 min at 13200 rpm at 4 °C. 4 µL of each sample were injected into the LC-MS system.

D6-chol levels were determined using a 1200 Series HPLC system (Agilent Technologies, Santa Clara, CA, U.S.A.) interfaced to an API 5500 triple quadrupole mass spectrometer (Sciex, Thornhill, Ontario, Canada). The mass spectrometer was equipped with an atmospheric pressure chemical ionization (APCI) source operating in positive ion and multiple reaction monitoring (MRM) mode to measure the product ions obtained in a collision cell from the protonated [M – H2O]+ ions of the analytes. The transitions identified during the optimization of the method were m/z 375.3–152.1 (quantification transition) and m/z 375.3–167.1 (qualification transition) for D6-chol; m/z 397.3–147.1 (quantification transition) and m/z 397.3–161.1 (qualification transition) for β-sitosterol (IS). D6-chol and beta-sitosterol were separated on a Gemini C18 column (50 × 2 mm; 5 µm particle size), using an isocratic gradient in 100% methanol at 35 °C.

Behavioral assessments

Behavior in mice was evaluated using Novel Object Recognition (NOR) test, Paw Clasping (PC) test, Grip Strength (GS) test, and Activity Cage (AC) test at 20, 29, 35, and 45 weeks of age for "early cohort" and "2 cycles cohort" and at 40 and 49 weeks of age for "late cohort".

Behavioral tests were conducted as described in (17). Rotarod (RR) test was performed at 46 weeks of age for "early cohort" and "2 cycles cohort" and at 50 weeks of age for "late cohort", as described in (17).

Fear Conditioning (FC) test was performed at 48 weeks of age for "early cohort" and "2 cycles cohort" and at 51 weeks of age for "late cohort". Contextual and cued fear conditioning were performed using the Fear Conditioning System (Ugo Basile, series 46000) according to the following protocol: on day 1, mice were transferred to the behavioral room 30 minutes before starting the test for the acclimation. Mice were then exposed to a conditioned stimulus (CS) consisting in a 10-second 3.5 kHz tone delivered 150 seconds after the beginning of the test. The unconditioned stimulus (US) was a 2-second 0.5 mA foot shock that terminated together with the CS. The conditioning was repeated 3 times, every 150 seconds. After the last conditioning, animals were returned to their own cage. On day 2, contextual memory was assessed by placing mice in the same conditioning chamber for 5 minutes. The freezing response was evaluated by measuring the number of freezing, total time of freezing and latency to freeze. On day 3, cued fear conditioning was assessed using a modified conditioning chamber obtained by attaching patterned contexts on the walls and floor. Once mice were placed in this modified chamber, the same protocol as of day 1 was applied, except for the electrical foot shock that was not administered. Number of freezing, time of freezing and latency to freeze were recorded. In the cued paradigm, the recording started 150 seconds after the beginning of the test, as the US was delivered at this point.

Y-maze test (YM) was performed at 30 and 48 weeks of age only for "2 cycles cohort". A Y-shaped maze with three arms at a 120° angle from each other was used. After placing the mice in the center of the maze, they had free access to all three arms. If the mice chose an arm than other than the one they come from, this choice was called an alteration, which was considered the correct response. On the contrary, returning to the previous arm was considered an error. The total number of arm entries and the sequence of entries were recorded in order to calculate the percentage of alternations according to the following formula: number of alternations / number of possible triads x 100.

For a summary of animals and the number of all the tests performed, see Supplementary Table 1.

muHTT aggregates analysis

Analysis was performed as described in (15). zQ175DN mice from "early cohort" were sacrificed at 29 or 50 weeks of age; zQ175DN mice from "late cohort" were sacrificed at 51 weeks of age; zQ175DN mice from "2 cycles cohort" were sacrificed at 50 weeks of age. Mice (n=3/group) were deeply anesthetized by ip injection of Avertin 2.5% and transcardially perfused with PFA 4%. Brains were post-fixed overnight in the same solution at 4°C and then in sucrose 30% to prevent ice crystal damage during freezing in OCT. Immunohistochemistry was performed on 15 µm coronal sections. Epitopes were demasked at 98°C with NaCitrate (10 mM, pH 6) for 15 minutes and then slices were blocked and permeabilized with Triton 0,5% and Normal Goat Serum 5% for 1h at RT. Subsequently, slices were immediately incubated with anti-EM48 primary antibody (1:100; Merck Millipore, cat n° MAB5374) for 3h at RT. Slices were washed 3 times (10 minutes each) with PBS + Triton 0.1% at RT and then anti-mouse Alexa Fluor 488-conjugated goat secondary antibodies (1:500; Invitrogen) were used for detection (1h at RT). Sections were counterstained with the nuclear dye Hoechst 33258 (1:10.000, Invitrogen), washed 3 times (10 minutes each) with PBS + Triton 0.1% at RT and then mounted under cover slips using Vectashield mounting medium (Vector Laboratories).

To count muHTT aggregates, confocal images were acquired with a LEICA SP5 laser scanning confocal microscope. Laser intensity and detector gain were maintained constant for all images and 5 to 10-z steps images were acquired at 40x. To count aggregates, 27 images/mice from 9 sections throughout the striatum and cortex were taken. To quantify the number and the size of aggregates, ImageJ software was used to measure the fluorescence. Images were divided into three-color channels and the same global threshold was set. "Analyze Particles" plugin (ImageJ) was used to count the number and the size of aggregates.

Isotope dilution-gas chromatography-mass spectrometry (ID-GC-MS) analysis for neutral sterols and 24S-OHC in brain tissues

Animals (n=4/group) were perfused with saline before to isolate the striatum and cortex to avoid blood contamination. Once isolated, brain tissues were frozen and kept at -80°C until their use. Frozen tissues were rapidly weighted and homogenized in ice with sterile PBS (400 µl for the striatum; 600 µl for the cortex) with an ultra-turrax homogenizer. In a screw-capped vial sealed with a Teflon-lined septum, 50 µl of tissue homogenates were mixed together with 500 ng of D4-lathosterol (CDN Isotopes), 500 ng of D6-desmosterol (Avantipolar Lipids), 100 ng of D6-lanosterol (Avantipolar Lipids), 400 ng of D7-24S-hydroxycholesterol (D7-24S-

OHC) (Avantipolar Lipids) and 100 µg of epicoprostanol (Sigma-Merck) as internal standards, 50 µl of butylated hydroxytoluene (BHT) (5 g/L) and 25 µl of EDTA (10 g/l). Alkaline hydrolysis was allowed to proceed at room temperature (22°C) for 1 h in the presence of 1 M ethanolic potassium hydroxide solution under magnetic stirring. After hydrolysis, the neutral sterols (cholesterol, lathosterol, desmosterol and lanosterol) and 24S-OHC were extracted twice with 5 ml of hexane. The organic solvents were evaporated under a gentle stream of nitrogen and converted into trimethylsilyl ethers with BSTFA-1% TMCS (Cerilliant) at 70°C for 60 min. Analysis was performed by GC–MS on a Clarus 600 gas chromatograph (Perkin Elmer) equipped with Elite-5MS capillary column (30 m, 0.32 mm, 0.25 µm. Perkin Elmer) connected to Clarus 600C mass spectrometer (Perkin Elmer). The oven temperature program was as follows: the initial temperature 180°C was held for 1 min, followed by a linear ramp of 20°C/min to 270°C and then a linear ramp of 5°C/ min to 290°C, which was held for 10 min. Helium was used as carrier gas at a flow rate of 1 ml/min and 1 µl of sample was injected in splitless mode. Mass spectrometric data were acquired in selected ion monitoring mode. Peak integration was performed manually. Sterols and 24S-OHC were quantified against internal standards, using standard curves for the listed sterols[16]. The weight of each sample was used to normalize raw data.

Electrophysiological analysis

Experiments were performed on submerged brain slices obtained from mice (n=3-4/group; 1-2 cells were recorded for each animal) at 53-55 weeks of age. Animals were anesthetized with isoflurane and transcardially perfused with ice-cold (<4°C), carboxygenated (95% O2 – 5% CO2) cutting solution (70 mM sucrose, 80 mM NaCl, 2.5 mM KCl, 26 mM NaHCO3, 15 mM glucose, 7 mM MgCl2, 1 mM CaCl2, 1.25 mM NaH2PO4). The brain was rapidly removed, and coronal slices (300 µm-thick) were cut at striatal level using a vibratome (DTK-1000, Dosaka EM, Kyoto, Japan). Slices were transferred into an incubating chamber filled with oxygenated ACSF (NaCl 125 mM, KCl 2.5 mM, NaHCO3 26 mM, Glucose 15 mM, MgCl2 1.3 mM, CaCl2 2.3 mM and NaH2PO4 1.25 mM) and allowed to equilibrate for 1 hour (30 minutes at 37°C and 30 minutes at room temperature). Slice were then transferred, one by one, to a submerged-style recording chamber for the whole-cell patch-clamp recordings. The chamber was mounted on an E600FN microscope (Nikon) equipped with 4× and 40× water

immersion objectives (Nikon) and connected to a near-infrared CCD camera for cells visualization.

Data were obtained from MSNs (6 cells from 3 wt mice; 8 cells from 4 zQ175DN mice; 5 cells from 3 zQ175DN+chol mice), identified by their basic membrane properties (membrane capacitance, input resistance, and membrane resting potential) and firing pattern (delayed regular firing). The patch pipettes were produced from borosilicate glass capillary tubes (Hilgenberg GmbH) by using a horizontal puller (P-97, Sutter instruments) and filled with an intracellular solution containing K-gluconate 130 mM, NaCl 4 mM, $MgCl_2$ 2 mM, EGTA 1 mM, creatine phosphate 5 mM, Hepes 10 mM, Na_2ATP 2 mM, Na_3GTP 0.3 mM (pH adjusted to 7.3 with KOH). The signals were amplified with a MultiClamp 700B amplifier (Molecular Devices) and digitized with a Digidata 1322 computer interface (Digitata, Axon Instruments Molecular Devices, Sunnyvale, CA). Data were acquired using the software Clampex 9.2 (Molecular Devices, Palo Alto, CA, U.S.A.), sampled at 20 kHz, and filtered at 2-10 kHz. The analysis of the membrane capacitance (Cm) and the input resistance (Rin) was performed using Clampfit 10.2 (Molecular Devices, Palo Alto, CA, U.S.A.). Cm was estimated from the capacitive current evoked by a -10 mV pulse, whereas Rin was calculated from the linear portion of the I-V relationship obtained by measuring steady-state voltage responses to hyperpolarizing and depolarizing current steps. The spontaneous excitatory postsynaptic currents (sEPSCs) – mediated by the activation of AMPA receptors as confirmed by their abolition following application of NBQX 10 μM – were recorded at a holding potential of -70 mV. Miniature EPSCs (mEPSCs) were derived in the presence of 1 μM TTX (Sigma-Aldrich). The off-line detection of the events was performed manually by using a custom-made software in Labview (National Instruments, Austin, TX, U.S.A.). The amplitudes of the events obeyed a lognormal distribution. Accordingly, the mean amplitude was computed as the peak of the lognormal function used to fit the distribution. Inter-event intervals (measured as time between two consecutive events) were distributed exponentially and the mean interval was computed as the tau value of the mono-exponential function that best fitted this distribution. The kinetic analysis of currents was performed by measuring rise time (time that current takes to activate from 10 to 90%) and time constant of decay (τd – time that current takes to deactivate exponentially to 37% of its peak value).

Bio-Plex analysis

To measure cytokines and chemokines, mice (n=4/group) were deeply anesthetized by ip injection of Avertin 2.5%. Blood was collected from the retro-orbital sinus in a tube containing 20 µL of heparin 2% and centrifuged at 4000 rpm in a bench-top centrifuge for 15 minutes to collect the plasma. Tissues (striatum, cortex, cerebellum, lung, liver, kidney, heart, and spleen) were isolated and frozen. 5 mg of each tissue were homogenized using a tissue grinder in 0.5 mL of lysing solution composed of 20 µL of factor 1, 10 µL of factor 2, 4995 µL of cell lysis buffer and 20 µL of PMSF 500 mM (Bio-Plex® Cell Lysis Kit, Biorad, #171304011). The lysate was frozen at -80°C for 2 minutes and then, following thawing on ice, it was sonicated at 40% for 20 seconds and centrifuged at 4500 rcf at 4°C for 4 minutes to collect the supernatant.

The supernatant was quantified using DC™ Protein Assay Kit I (Biorad, #5000111) and samples were diluted to a final concentration of 500 µg/mL. To perform the Bio-Plex assay, 150 µL of assay buffer were added to 150 µL of samples. Concerning the plasma, samples were centrifuged at 1500 rcf at 4°C for 5 minutes. 60 µL of assay buffer and 120 µL of sample diluent were added to 60 µL of plasma.

Cytokine levels were measured by using a Bio-Plex murine cytokine 23-Plex assay kit (Biorad, #M60009RDPD) which evaluated the levels of: Eotaxin, IL-1a, IL-1b, IL-2, IL- 3, IL-4, IL-5, IL-6, IL-9, IL-10, IL-12(p40), IL-12(p70), IL-13, IL-17, TNF-alpha, granulocyte colony-stimulating factor (G-CSF), granulocyte/macrophage colony-stimulating factor (GM-CSF), IFN-gamma, KC, RANTES, macrophage inflammatory protein (MIP-1a and MIP-1b) and monocyte chemotactic protein-1.

Briefly, magnetic beads were added to a 96-well plate which was fixed on a handheld magnetic washer. Samples were added and the plate was shacked at 300 rpm for 30 minutes at room temperature. After 3 washing steps, detection antibodies were added, and the plate was shacked at 300 rpm for 30 minutes at room temperature. After 3 washing steps, streptavidin-PE was added, and the plate was shacked at 300 rpm for 10 minutes at room temperature. After 3 washing steps, assay buffer was added and the cytokines levels were read on the Luminex 200 System, Multiplex Bio-Assay Analyzer and quantified based on standard curves for each cytokine in the concentration range of 1–32,000 pg/mL. The analytes concentrations specified for the eight-point standard dilution set included in the kit have been selected for optimized curve fitting using the five-parameter logistic regression in Bio-Plex ManagerTM software.

These curves were used to interpolate the measured concentration. Data were normalized over the mean of the wt group.

In vivo evaluation of safety: hematology, clinical chemistry, and histopathology

17 mice (6 wt; 6 zQ175DN; 5 zQ175DN+chol) from "2 cycles cohort" underwent pathological evaluation to exclude adverse effects of the treatment. Mice were sacrificed at 50 weeks of age. Peripheral blood was sampled from the retro-orbital sinus and collected in Eppendorf Tubes® containing 20 µL of Heparin 2%. Blood samples were analyzed by means of a laser-based hematology analyzer (Sysmex XT-2000iV, Kobe, Japan). Blood smears were also prepared, stained with May Grunwald Giemsa and examined. Plasma obtained from blood samples was used to measure biochemical analytes by means of an automated spectrophotometer (BT3500, Biotecnica Instruments SPA, Rome, Italy). The following analytes were measured: cholesterol, triglycerides, glucose, total protein, albumin, creatinine, ALT and AST.

A complete necropsy was also performed. The total body weight was recorded, along with the weight of liver, spleen, kidneys, heart, and testes. The weight of the organs was normalized for the total body weight. Femoral bone marrow smears were also prepared, stained with May Grunwald Giemsa and examined. The following organs were collected and routinely processed for histopathology: brain, heart, lungs, liver, kidneys, spleen, salivary glands with mandibular lymph nodes, skin, skeletal muscle, testes, uterus, and ovaries. Hematoxylin and Eosin slides were examined by two pathologists blinded to the treatment groups.

PCA analysis

Principal component analysis at 29 weeks of age and 45-49 weeks of age was done using the built-in R function prcomp() and visualized using factoextra (version 1.0.7). At 29 weeks of age, the PCA was performed using the following variables: Nor, Paw Clasping, Grip Strength, Activity Cage (global) and Activity Cage (distance). At 45-49 weeks of age, two more variables (Rotarod and Fear Conditioning) were considered. The ellipses were calculated with a 95% confidence interval around the centroid of each group.

Statistics

G*Power (https://www.psychologie.hhu.de/arbeitsgruppen/allgemeine-psychologie-und-arbeitspsychologie/gpower) was used to compute statistical power analysis in order to pre-determine group allocation, data collection, and all related analyses. Prism 8 (GraphPad software) was used to perform all statistical analyses. Data are presented as mean±standard error of the mean (mean±SEM). The limit of statistical significance was set at p-value < 0.05. Grubbs' test was applied to identify outliers. For each set of data to be compared, we determined whether data were normally distributed or not to select parametric or not parametric statistical tests. The specific statistical test used is indicated in the legend of the figures.

Data availability

This study does not include data deposited in public repositories. Data are available on request to the corresponding authors.

Results

In vivo distribution and pharmacokinetics of hybrid-g7-NPs-chol

To design the therapeutic regimens for hybrid-g7-NPs-chol, we first tracked the temporal dynamic of the intracellular release of cholesterol from NPs by using hybrid-g7-NPs tagged with Cy5 (a far-red fluorescent dye) and loaded with bodipy-cholesterol, a photostable fluorescent cholesterol derivative. The overlap coefficient between the Cy5 (detecting the NPs) and bodipy (tracking the cholesterol moiety) signals measured by confocal microscopy was then used to assess the release of cholesterol from the NPs.

7 weeks-old wt mice were treated with a single ip injection, sacrificed at 24 hours, 2, 10, and 20 weeks and overlap coefficient measured over time on the cryo-sectioned brain slices (Supplementary Fig. 1A). We found that 24 h after a single ip injection, Cy5 and bodipy signals colocalized in striatum and cortex (overlap coefficient = 0.829 and 0.758 respectively; an overlap coefficient of 1 indicates total overlap) (Supplementary Fig. 1B and C), while 2 weeks later the two signals were partially separated (Supplementary Fig. 1B and C). Overlap coefficient at 2 weeks showed that approximately 30% of bodipy no longer colocalized with Cy5 in cortex and striatum, suggesting a progressive release of cholesterol from the NPs, in

parallel with a reduction in Cy5 signal probably due to polymer degradation (overlap coefficient = 0.708 in striatum and 0.542 in cortex; Supplementary Fig. 1B and C). At 10 weeks post injection, 70% of cholesterol was released in the striatum and 63% in the cortex (overlap coefficient = 0.232 and 0.274 respectively), while at 20 weeks 93% of cholesterol was released in the striatum and 86% in the cortex (overlap coefficient = 0.057 and 0.109 respectively; Supplementary Fig. 1B and C). Collectively, these data show that, in the brain, all encapsulated cholesterol is released within 20 weeks.

To strengthen our understanding of NPs pharmacokinetics and quantify the amount of exogenous cholesterol reaching the brain, we exploited deuterated cholesterol-laden hybrid-g7-NPs (hybrid-g7-NPs-d6-chol) (Supplementary Fig. 1D). The presence of six deuterium atoms in the cholesterol structure allowed us to distinguish exogenous from endogenous cholesterol and to quantify the former by mass spectrometry in different tissues[17]. Our hybrid-g7-NPs-chol carried a calculated amount of about 29 mg of cholesterol for 100 mg of NPs (see also Methods). In our previous study we showed that the concentration of d6-chol in different brain regions (striatum, cortex, cerebellum) at 24 hours was between 0.36 and 0.54 ng/mg of tissue, with values increasing up to three times at the 2-week time point (described in 17, summarized in Supplementary Table 2). In Supplementary Table 2 we have now added the time points 10- and 20-weeks post ip injection (red boxes in Supplementary Table 2). We found that d6-chol was still present in the brain at 10 weeks even though the amount was halved compared to 2 weeks, with a further reduction observed at 20 weeks and levels returning to those seen 24 hours after treatment. Importantly, the amount of d6-chol in peripheral tissues and plasma decreased over time and was no longer detected at the late time points, suggesting that cholesterol was used by brain cells and cleared in the periphery (Supplementary Table 2).

A one cycle of treatment in pre-symptomatic stages produces solid but transient benefits in zQ175DN mice

To test the long-term efficacy and safety of hybrid-g7-NPs-chol we employed the slow-progressing zQ175DN mouse model in a C57BL6 background. In our first experimental paradigm, which we called the “early cohort”, pre-symptomatic zQ175DN mice were ip injected with hybrid-g7-NPs-chol from 5 to 9 weeks of age (herein named zQ175DN+chol), using the same experimental paradigm described in (17) and also adopted for the injection of the earlier g7-PLGA-NPs-chol formulation in R6/2 mice[14], i.e. 2 injection/week for 5 weeks.

Since about 493 µg of cholesterol was administered with each ip injection (see methods), a cycle of 10 ip injections corresponded to a total of about 4930 µg of cholesterol administered to each animal. This amount was about 30 times higher than the amount used in the previous study with g7-PLGA-NPs-chol[14]. We also calculated that since 10% of NPs are expected to pass the BBB due to the g7 peptide[14,16], the amount of cholesterol that reached the brain was approximately 493 µg for a cycle of treatment, a dose similar to the higher one delivered into the striatum with the osmotic mini-pumps, which led to improvement of both cognitive and motor defects in the R6/2 mice[15]. As controls in these trials, wt and zQ175DN mice were treated with saline solution (herein named wt and zQ175DN, respectively). Cognitive and motor skills were extensively assessed in each group at 20, 29, 35 and 45-48 weeks of age (Fig. 1A; Supplementary Table 1).

To assess cognitive performance, we first ran the Novel Object Recognition (NOR) test, which measures recognition memory, a subtype of long-term declarative memory, and is based on rodents' natural propensity to explore novelty. Recognition memory was severely impaired in zQ175DN mice as early as 20 weeks of age and the defect persisted up to the tested 45-week time point (negative Discrimination Index in Fig. 1B). Upon pre-symptomatic treatment, zQ175DN mice no longer showed this anomaly at the 20 and 29 weeks of age but the effect was lost at 35 and 45 weeks (Fig. 1B). This finding is consistent with the kinetics of cholesterol release, accumulation, use and elimination in the brain as described in Supplementary Figure 1 and in Supplementary Table 2.

At 48 weeks of age, we also performed the Fear Conditioning (FC) test, a type of associative learning task that measures the ability to storage and retrieve information resulting from an association with other information. In this test mice learn to associate a neutral conditional stimulus (tone) with an aversive unconditional stimulus (a mild electrical foot shock) and show a conditional fear response which is absence of movement (freezing). We found that zQ175DN mice exhibited a reduced number of freezing in both contextual (when the animal is tested in the original training context) and cued (when the conditional stimulus is presented in a different context) paradigm, but the cholesterol treatment was not sufficient to reverse this defect (Supplementary Fig. 2A and 2B).

To assess the impact of exogenous cholesterol on disease progression, we also measured dystonic movements through the Paw Clasping (PC) test. zQ175DN mice manifested clasping activity as early as 20 weeks of age, which was not rescued in zQ175DN+chol mice (Fig. 1C).

However, at 29 weeks of age, the amount of cholesterol released by the NPs was sufficient to normalize clasping behaviour. As for the NOR, this effect was lost at 35 and 45 weeks of age (Fig. 1C).

In the Grip Strength (GS) test, which measures neuromuscular strength, zQ175DN mice showed a defect in this parameter compared to controls at all time points (Fig. 1D). The delivery of cholesterol to the brain of these mice completely reversed this defect at 20 and 29 weeks of age, but at 35 weeks the improvement was markedly diminished although still significant and was lost at 45 weeks (Fig. 1D).

At 46 weeks of age, Rotarod (RR) test was used to assess motor skills. A decrease in the latency to fall in zQ175DN mice compared with wt littermates was observed, confirming the late-onset motor defect observed in this mouse model. However, this late defect was not recovered by the pre-symptomatic treatment (Fig. 1E).

These data indicate that the pre-symptomatic manifestations of the disease regressed until week 29 (NOR and PC test) or week 35 (GS test) in the treated animals, i.e. 20-26 weeks after the last injection depending on the measured parameter.

Treatment is effective also at symptomatic stages

In a second experimental paradigm, called “late cohort”, we tested the capacity of hybrid-g7-NPs-chol to counter the manifestations of the disease in symptomatic zQ175DN mice treated from 25 to 29 weeks of age with the same therapeutic regimen used above (Fig. 1F). At 40 and 49 weeks of age, zQ175DN+chol mice showed a complete rescue of cognitive decline, evaluated with NOR test, compared to the corresponding saline-treated zQ175DN mice (Fig. 1G).

Regarding the PC test, we found that at 49 weeks of age, zQ175DN+chol mice performed better than wt and zQ175DN groups (Fig. 1H) although in this (smaller) study at both 40 and 49 weeks we were not able to see a significant difference between the last two groups, as with age the wt mice also developed clasping. zQ175DN+chol mice showed also complete rescue of neuromuscular defects at both 40 and 49 weeks of age compared to zQ175DN mice, i.e. also at the 49 weeks’ time point that was not rescued in the “early cohort” (Fig. 1I and 1D). In contrast, while cholesterol administration at presymptomatic stage was not effective in the RR

test (Fig. 1G), zQ175DN mice of the "late cohort" group showed improved performance in this test at 50 weeks of age (Fig. 1J).

The combination of early and late cholesterol administration leads to complete cognitive and motor recovery

The finding that the beneficial effect of one cycle of treatment persisted at 29 weeks of age (20 weeks after the last ip injection, Fig. 1B-D) but was lost from 35 weeks of age, suggested that more cycles of treatment are needed to maintain the benefit over time. Consequently, we tested the combination of two cycles of treatment, the first from 5 to 9 weeks of age (as performed with the "early cohort", Fig. 1A) and the second from 21 to 25 weeks of age for a total of 20 injections per animal ("2 cycles cohort"; Fig. 2A).

Importantly, a sustained, robust, and reproducible therapeutic effect on cognitive and motor defects was observed in zQ175DN mice after two cycles of hybrid-g7-NPs-chol and up to the study endpoint of 45-50 weeks of age. Cognitive decline associated with recognition memory was completely prevented in zQ175DN+chol mice at all time points (Fig. 2B). Two cycles of hybrid-g7-NPs-chol also normalized the reduced number of freezing observed in zQ175DN mice exposed to the cued paradigm in the FC test (Fig. 2C), but not in the contextual paradigm (Supplementary Fig. 2C). To explore further aspects of cognition, we also performed the YM spontaneous alternation test, which measures the rodents' willingness to explore new environments and provides an index of their short-term memory. This test revealed no difference at 30 and 48 weeks between the genotypes (Supplementary Fig. 2D).

Disease progression, as assessed by the PC test, was halted in the 2 cycles treated zQ175DN+chol mice starting at 29 weeks of age and improvement remained highly significant at 35 and 45 weeks of age (Fig. 2D). In contrast, at the same time points, the "early cohort" showed no recovery in the NOR and PC tests (Fig. 1B-C). Even in the GS test, where the efficacy of one cycle treatment in the "early cohort" at 35 weeks of age was moderately present and then lost at 45 weeks of age (Fig. 1D), the "2 cycles cohort" showed a complete recovery that was highly significant at all late time points analysed, with values overlapping those of wt mice (Fig. 2E).

Regarding motor defects, two cycles of hybrid-g7-NPs-chol normalized RR performance in zQ175DN+chol mice compared to untreated mice, reaching values similar to those observed in wt mice (Fig. 2F).- Regarding other motor skills (assessed by the Activity Cage test, AC), a small, but significant, reduction in global activity and total distance travelled was found at 45

weeks of age compared to wt mice and the administration of cholesterol was able to counteract these defects (Fig. 2G and 2H). These benefits were not observed in the zQ175DN+chol mice from the "early" and "late" cohorts (Supplementary Fig. 2E-H).

Figure 3A shows the heat-maps generated by aggregating the values of the cognitive and motor tasks of all cohorts of animals and using a system of color-coding to represent different levels of performance (green, good performance; red, bad performance). As expected, zQ175DN mice worsened over time across all tests, while zQ175DN+chol mice from the "early cohort" performed much better for 20 weeks after the last ip injection (29 weeks' time point), compared to their HD littermates (Fig. 3A, heat-map, top). However, two cycles of treatment ("2 cycles cohort"; Fig. 3A, heat-map, center) were required to have a complete and lasting recovery. The third heat-map (Fig. 3A, bottom) summarizes the HD-related defects recovered in the "late cohort" cholesterol treated mice.

Principal component analysis (PCA) of all values related to motor and cognitive tests for all tested paradigms, also clearly separated the wt groups from the zQ175DN groups (Fig. 3B-C). Importantly, at 29 weeks of age, the zQ175DN+chol group of the "early cohort" clearly separated from the zQ175DN group and showed an overlap with the age-matched wt group (Fig. 3B). Similarly, at 45-49 weeks of age, zQ175DN+chol mice from the "late cohort" and zQ175DN+chol mice from the "2 cycles cohort" were distinguishable from the zQ175DN group and partially overlapped with wt group (Fig. 3C). On the contrary, zQ175DN+chol group from the "early cohort" was similar to the zQ175DN group at this late time point, as highlighted by the behavioural analysis (Figures 1 and 2).

To explore further the impact of cholesterol delivery on cognitive decline in HD, we collected all raw data obtained in the NOR tests performed on R6/2[17] and zQ175 (this paper) mice injected ip with hybrid-g7-NPs-chol, and from R6/2 mice treated with g7-PLGA-NPs-chol[14] or implanted with cholesterol-filled osmotic mini-pumps[15] or injected intracerebrally with AVV-SREBP2[20]. For all these studies only the last time point was considered for a total of 124 wt (control) mice, 130 HD untreated mice and 127 HD treated mice (the latter two groups included both R6/2 and zQ175 mice) that were statistically compared. As shown in Fig. 3D, the distribution of the NOR values from HD mice treated with any of the treatments mentioned above, including those used in this paper, regardless of the type of strategy, delivery system, mouse line and time of administration, overlapped more with the values of the wt groups than those of the HD groups, highlighting the consistency of any cholesterol-raising treatment in

countering cognitive decline in HD. In the present study we demonstrate that the administration of cholesterol to the brain can lead to recovery from cognitive dysfunction lasting nearly 1 year.

We also evaluated the level of cholesterol, of key cholesterol precursors lanosterol, lathosterol, and desmosterol, and of the brain-specific cholesterol catabolite 24S-OHC in all zQ175DN mice at the two endpoints of the different therapeutic regimens used in the current study (i.e. at 29 and 50-51 weeks) (Fig. 4; Supplementary Fig. 3 and 4). A robust deficit in the amount of cholesterol (in striatum), lanosterol, lathosterol, and desmosterol, and 24S-OHC (in striatum and cortex) was found in zQ175DN mice compared to wt mice, confirming previous results obtained in other HD models[5,20] and in the Q175 mice[7] (in the study by Shankaran et al., the Q175 mice used carried the floxed neo cassette). However, systemic administration of hybrid-g7-NPs-chol did not modify the steady-state levels of all the metabolites in both striatum (Fig. 4; Supplementary Fig. 3) and cortex (Supplementary Fig. 4).

Taken together these data demonstrate that one cycle of hybrid-g7-NPs-chol treatment, either at pre-symptomatic or symptomatic stage, is sufficient to prevent or normalize several behaviour defects for a long time, but two cycles of hybrid-g7-NPs-chol are necessary to obtain lasting and complete therapeutical benefits.

Exogenous cholesterol also ameliorates the neuropathological deficit of HD mice

The evidence that exogenous cholesterol produces lasting benefits in zQ175DN mice led us to investigate whether early and late neuropathological dysfunctions typical of the disease state were also improved. Our previous work demonstrated that 4-week infusion of 369 µg of cholesterol with osmotic minipumps into the striatum of the rapidly progressing R6/2 mouse model reduced the number and size of muHTT aggregates present from birth[15].

At 29 and 50 weeks of age, zQ175DN mice exhibited muHTT aggregates as detected using EM48 antibody (Fig. 5). In contrast, zQ175DN+chol mice that received one cycle of hybrid-g7-NPs-chol at pre-symptomatic stage ("early cohort", Fig. 5A) show a statistically significant reduction in the number of muHTT aggregates in both striatum and cortex at 29 weeks of age, i.e. 5 months after the last ip injection, and this effect was lost at 50 weeks (Fig. 5B-C and E-F). In the cortex (Fig. 3G), where more NPs are known to accumulate[17], but not in striatum (Fig. 5D), the size of muHTT aggregates was also reduced at 29 weeks in cholesterol treated animals, an effect that even in this case was lost at 50 weeks of age, consistent with the

behavioural data described in Figure 1. When the hybrid-g7-NPs-chol was administered in symptomatic zQ175DN mice ("late cohort"; Fig. 5H), the number and size of muHTT aggregates were significantly reduced both in striatum and cortex of 50-week-old HD mice (Fig 5I-N). These sets of data indicate that exogenous cholesterol rather than preventing aggregates formation, favours their clearance. Of note, the 50-week-old zQ175DN+chol mice that received two cycles of hybrid-g7-NPs-chol ("2 cycles cohort"; Fig. 5O) showed a larger reduction in the number and size of muHTT aggregates in both striatum and cortex compared to zQ175DN control mice (Fig. 5P-U).

All these findings demonstrate that cholesterol delivery to the HD brain through systemic injection of hybrid-g7-NPs-chol efficiently reduces muHTT aggregation, but the content and timing of the treatment are critical for detecting changes.

Neuronal functionality is restored by two cycles treatment

Excitatory synaptic transmission is known to be severely affected in MSNs from different HD mouse models[22-24]. Increased input resistance (Rin) and decreased frequency of spontaneous excitatory post-synaptic currents (sEPSC) were described in MSNs of Q175 mice carrying the neo cassette compared with MSNs of wt mice[23-26].

Here we examined the electrophysiological properties of striatal MSNs from brain slices of wt and zQ175DN mice versus those of zQ175DN+chol mice of the "2 cycles cohort". The analysis of the basic membrane properties of MSNs did not show difference in membrane capacitance (Cm) between genotypes (Fig. 6A). Instead, the resting membrane potential (Vm) was significantly depolarized, and membrane Input Resistance (Rin) was increased in zQ175DN MSNs with respect to wt MSNs (Fig. 6B and C). Notably, NPs-based cholesterol delivery normalized Vm in zQ175DN+chol MSNs bringing the value back to those of wt MSNs (Fig. 6B).

We also demonstrated that the frequency of spontaneous and miniature AMPA-mediated excitatory postsynaptic currents (sEPSC and mEPSCs respectively) was reduced in zQ175DN MSNs compared to those of wt MSNs, as reported by their higher mean inter-event interval (inverse of the frequency) (Fig. 6D-F). Of note, these electrophysiological changes were completely rescued in zQ175DN+chol MSNs (Fig. 6D-F). Moreover, the cumulative inter-event interval curve indicated that the distribution of the inter-event intervals of the sEPSCs

and mEPSCs in the zQ175DN+chol MSNs overlapped that of wt MSNs (Fig. 6G-H). No significant differences in the average amplitude and kinetics (rise time and decay time) of the sEPSC (Supplementary Fig. 5A-C) and the mEPSCs (Supplementary Fig. 5D-F) were found between the three groups of MSNs.

These data indicate that the hybrid-g7-NPs-chol formulation restores synaptic function in zQ175DN MSNs and that behavioral improvement correlates with the normalization of electrophysiological parameters.

Absence of long-term side effects of the treatment regimen

We also assessed the likelihood that "two cycles" of hybrid-g7-NPs-chol could cause noticeable side effects. A multiplex immunoassay (Bio-Plex) was used to simultaneously measure the level of 23 inflammatory cytokines in several tissues (striatum, cortex, cerebellum, lung, liver, kidney, heart, spleen) and in plasma. By comparing the values of the different analytes in 9 different tissues specimen from wt and zQ175DN mice with zQ175DN+chol mice, we found an overall similar inflammatory profile between the groups with slight modifications for only 2 pro-inflammatory analytes (eotaxin an KC) in three tissues (striatum, cerebellum, and liver), suggesting that the treatment does not induce a relevant immune response (Supplementary Table 3).

Clinical observation of mice exposed to the different therapeutic regimens also revealed no cases of mortality in the groups nor did routine hematology reveal any differences between the groups (Supplementary Table 4). Platelet count was higher in the zQ175DN+chol group compared to wt ($p = 0.028$) and zQ175DN ($p = 0.011$) groups. However, large platelet clumps were detected on smears from the latter groups (wt, 2/6 mice; zQ175DN, 4/6 mice). A statistically significant difference in albumin concentration was detected between the zQ175DN+chol mice and wt mice ($p = 0.019$), and between zQ175DN+chol mice and zQ175DN mice ($p = 0.025$) (Supplementary Table 5). Overall, these data indicate good *in vivo* tolerability of two cycles of hybrid-g7-NPs-chol.

No statistically significant difference in the total body weight and in the weight of organs was found between zQ175DN and zQ175DN+chol groups (Supplementary Table 6). No major histopathological findings were detected in any of the organs examined (Supplementary Table 7) and those occasionally present were interpreted as background or incidental lesions with no

differences in their frequency or severity among groups. In all cholesterol treated mice from the "2 cycles cohort", numerous (5-6 per mouse), spherical, 2 to 3 mm in diameter, whitish, hard concretions were found free in the abdominal cavity. No gross lesions associated to the concretions were observed. Histological examination of these concretions revealed a central mineralized core, admixed with necrotic material, cholesterol clefts, variable number of foamy macrophages and occasional multinucleated giant cells, surrounded by a fibrous capsule (foreign body granuloma) and externally lined by a monolayer of flattened mesothelium. These concretions were not or rarely present in the other therapeutic regimens (in "early cohort" and "late cohort") and their number and size were dependent on the timing and number of cycles (Supplementary Table 8).

Discussion

There is now overwhelming evidence to support the fact that raising the cholesterol level and/or targeting its homeostasis in the brain of HD mice can halt disease progression. In our initial works, we delivered cholesterol to the brain of R6/2 mice through nanoparticles[14,17] or osmotic mini-pumps[14] and more recently through nose-to-brain delivery (ref). In an additional strategy we and others focused on a gene therapy approach. In one study an AAV vector was used to overexpress the neuronal-specific CYP46A1 gene in the striatum of R6/2 and zQ175DN mice[6,27]. Since CYP46A1 catalyzes cholesterol into 24S-OHC, which then binds to LXR and stimulates cholesterol synthesis in glial cells, this approach resulted in the promotion of cholesterol metabolism and amelioration of motor deficits in HD mice[6,27]. In a further gene therapy approach we expressed the active form of the SREBP2 gene in R6/2 striatal astrocytes *in vivo*, as this transcription factor promotes the transcription of genes in the cholesterol biosynthesis pathway[20]. All these approaches improved neuronal function and alleviated phenotypes in HD mice, in agreement with the evidence that contrasting reduced cholesterol biosynthesis and CYP46A1 and SREBP2 activity in the HD brain is beneficial.

Here, we have expanded these therapeutic options by providing evidence of the long-term beneficial effect of second-generation NPs-based cholesterol administration in countering cognitive decline, disease progression, motor defects, and neuropathological signs in the slow-progressing zQ175DN mouse model. We show that the established treatment regimen is effective when administered in pre-symptomatic or symptomatic stages. In particular, comparing an "early" (pre-symptomatic) with "late" (symptomatic) treatment regimen or a

combination of both ("two cycles") over the course of nearly 1 year, we show that efficacy of the cholesterol treatment persists for 5 months after the last injection, regardless of the time of administration. We also show that its effectiveness can be extended beyond 40 weeks (10 months) with two treatment cycles, therefore culminating in a long-lasting recovery.

In our study, we employed the zQ175DN mouse model in a C57BL6 background and further characterized its early disease stages. Previous data on these mice, in an FVB background, described the first sign of cognitive and motor deficits starting from 6-9 months[17]. Here we show that cognitive decline, neuromuscular (grip) defects, and functional deterioration begin at 5 months (20 weeks) of age, a time point that can be considered similar to the onset of a prodromal phase in human that is also characterized by cognitive changes and grip abnormalities[28-30].

Cognitive impairments are often reported as the most debilitating aspect of HD that is currently not being treated. In our study, we show that the alleviation of cognitive decline as measured by the NOR test in zQ175DN mice occurs with all therapeutic regimens (i.e. in the "early", "late" or "2 cycles" cohorts) but is long-lasting only with the "2 cycles" treatment. In fact, in the "early" therapeutic regimen, efficacy is maintained up to 29 weeks of age, i.e. 20 weeks after the last ip injection, and is reduced and then lost after 35 weeks of age. These data, together with Cy5-Bodipy imaging data, concur to establish that the release of cholesterol from injected NPs is complete in 5 months and that an additional course of treatment is required for a lasting effect in brain.

Another type of memory we tested in our cholesterol delivery strategy is associative memory, as measured by the FC test. Here the rescue in the freezing behavior of zQ175DN mice was only observed in the "2 cycles cohort", indicating that a sustained treatment of cholesterol is needed. We also report that while at 20 weeks of age the "early cohort" shows a rescue in the NOR test, the clasping behavior - a measurement of motor defect - is recovered at a later time point, i.e. at 29 weeks of age, consistent with our earlier data showing that motor recovery requires the release of a higher dose of cholesterol[15], and is then maintained at later time points only with the "2 cycles" treatment.

Recognition memory and associative memory in mice recruit both the hippocampus and surrounding regions of the cortex, but recognition memory is mainly associated to the cortico-striatal pathway[23,32,33]. On the contrary, amygdala is mostly involved in the FC-dependent associative memory[34]. The stronger effect in NOR performance with respect to FC performance

observed in zQ175DN mice following ip injection of hybrid-g7-NPs-chol suggests that exogenous cholesterol primarily acts on cortico-striatal and hippocampal-striatum interactions[35]. These findings support the value of strategies aimed at increasing cholesterol biosynthesis as modifier of cognitive symptoms that appear in the early phases of the disease. Importantly, the evaluation of cognitive performance assessed by NOR test in all cholesterol-raising trials performed so far in HD mice (total 381 mice and measurements) - with the only exception of the two AAV-CYP46AI mouse trials which measured only motor performance[6,27] - demonstrated that regardless of the treatment, animal model, and time of administration, providing exogenous cholesterol or/and increasing cholesterol biosynthesis in the brain of HD mice is a therapeutic option.

Our previous studies have shown that 15-20 µg of cholesterol (administered with g7-PLGA-NPs-chol[14] or with minipumps[15]) are sufficient to obtain a complete prevention of cognitive decline and that higher doses of cholesterol maintain this benefit[15]. In this study, we confirmed that the dose of cholesterol necessary to prevent or rescue cognitive decline in HD mice is rather low, thus anticipating that a wide window of therapeutic intervention is available on the cognitive aspect. With respect to motor defects, our data also support the published literature demonstrating that a high dose of cholesterol is needed to restore the motor-dependent circuits[15]. Accordingly, full recovery in the AC and RR tests coincided with the complete release of cholesterol from the NPs while normalization in PC was maximal only when release was at its highest values (at 29w).

We also report that administration of cholesterol through hybrid-g7-NPs-chol normalizes Vm value and partially rescues Rin deficit. The depolarization of Vm in zQ175DN MSNs and its recovery in the cholesterol treated mice probably involve ATP-dependent mechanisms which are closely related to the functionality of the Na+-K+-ATPase[36,37]. Our data also suggest that exogenous cholesterol acts pre-synaptically. In fact, its administration normalizes the frequency of mEPSCs, which reflects the probability of stochastic release of synaptic vesicles from the presynaptic terminals and is also related with the number of synapses/active zones. These findings support the notion that efficacy of exogenous cholesterol may also rely on its ability to restore synaptic defects in HD. A deeper understanding of the specific cell- and circuit-based signals associated with the behavioral recovery observed in treated mice will help increase knowledge about the biology of cholesterol-based recovery and future advances in nanotechnology.

Extensive mass spectrometry-based studies demonstrated that cholesterol biosynthesis is early reduced in the HD brain and across different rodent models[4-7,21,27]. We confirmed a decrease in the steady-state level of cholesterol in striatum of zQ175DN mice. Cholesterol precursors and its major catabolite, 24S-OHC, are also reduced in the striatum and cortex of zQ175DN mice compared to wt mice. In our previous studies, a high dose of cholesterol infused directly into the striatum of R6/2 mice enhanced biosynthesis of endogenous cholesterol[15], possibly through its conversion to 24S-OHC in neurons that in turn stimulates cholesterol synthesis in the glial cells. In this study, we did not detect an increase in the steady-state levels of cholesterol precursors and 24S-OHC levels suggesting that endogenous cholesterol synthesis is not modulated in the treated animals. However, these measurements were only performed at a single late time point, i.e. 20w after the last injection.

Our previous results in R6/2 mice showed that cholesterol infusion[15] or enhancement of endogenous cholesterol biosynthesis[20] in the striatum promotes clearance of muHTT aggregates. Here we confirm this finding in zQ175DN mice and demonstrate that treatment in presymptomatic stages reduces the number of aggregates in the striatum and cortex while late treatment is effective on both number and size of the aggregates. With two treatment cycles, muHTT aggregates are barely present in both the striatum and cortex, suggesting that more cycles produce a greater and longer beneficial effect, and that exogenous cholesterol probably acts to increase muHTT clearance. The significant correlation between muHTT aggregates and cognitive decline, disease progression and neuromuscular defects, suggests that clearance of muHTT aggregates after cholesterol administration may explain the animal's behavioural improvement.

Finally, our analyses of inflammatory status and complete necropsy performed on "2 cycles cohort" mice showed no significant changes or treatment-related lesions indicative of a side effect. The intra-abdominal mineralized concretions observed in the zQ175DN+chol group are likely a foreign body reaction to ip administration of the formulation in mice and have therefore limited translational significance[38,39]. Differences in platelet count are expected to be a preanalytical artifact induced by platelet clumping, which was frequently observed in the wt and zQ175DN groups, and not in the zQ175DN+chol group. Similarly, the higher albumin concentration measured in the zQ175DN+chol group can be interpreted as a nonspecific finding, possibly due to moderate dehydration.

In summary, our results obtained by analyzing behavioral and neuropathological parameters on a total of 49 zQ175DN mice treated with cholesterol compared to 48 wt and 48 zQ175DN mice, support the therapeutical potential of cholesterol-based nanomedicine as a modifier of disease progression during prodromal or symptomatic stages. We also show that two cycles of cholesterol administration led to a complete and prolonged recovery of cognitive and motor deficits that lasts for nearly one year. Furthermore, the slow release of exogenous cholesterol by the NPs can mimic the low and constant daily synthesis of cholesterol that occurs physiologically in the adult brain.

Since the robustness of the therapeutical impact of cholesterol delivery to the HD brain, the next challenge is now to optimize further these nanodrugs to bring and release the ideal amounts of cholesterol in the human brain over time through routes of administration that are closer to clinical application, compared to ip administration. One promising strategy may rely on intranasal delivery of nanoparticles or liposomes, as more recently proposed[19]. The optimization of this nose-to-brain delivery strategy may help to overcome the BBB and easily deliver cholesterol to the brain. Furthermore, the new nano-products should have all the characteristics required by the market to cross the preclinical-clinical boundary and become a true therapy for HD patients.

Acknowledgements

The authors acknowledge Dr. Stefania Antonini, delegate of the University of Milan for the animal care, the designed veterinarians and the Charles River technical personnel of the animal facility located at L.I.T.A. (Segrate) for their support in the management of mouse colonies, and Prof. Flavia Antonucci and Dr. Clara Cambria for advice about YM test.

Funding

The financial support of Fondazione Telethon - Italy (Grant no. GGP17102) is acknowledged (2018-2021); this work has was also partially supported by the European Union Circ Prot 643417 _Project within the framework of the Joint Call (JPND), with funding from the corresponding JPND National Funding Agencies; and by the European Union's Horizon 2020 Research and Innovation Programme under grant agreement No 874758 - Consortium "NSC-Reconstruct: Novel Strategies for Cell based Neural Reconstruction" (2020-23).

Competing interests

The authors report no competing interests.

Author contributions

MV, GB and EC conceived the study; GB managed the colonies and performed the treatments; GB and MV designed the treatment regimens, performed behavioral tests, sacrificed mice and collected tissues for all the subsequent analyses; IO, BR, JTD, MVa, RC, GT prepared and characterized all the NPs used in the study and contributed to the design of in vivo experiments; GB performed immunostaining experiments and provided confocal images and quantification; MRN performed the PCA analyses and metadata analysis of cognitive task in different trials; FT and GBi performed and analyzed the electrophysiological recordings; CC, FT and VL performed and analyzed mass spectrometry experiments; AP, MF, LC, RB and MS performed and analyzed mass spectrometry analysis for d6-chol quantification; ES, AC, LM performed histopathology and SP performed hematology and clinical chemistry; MV and GB collected study data and performed statistical analysis; MV and EC oversaw and coordinated responsibility for all research activities and their performance and provided experimental advice throughout the work. EC secured the fundings and the execution of the entire project. MV, GB and EC wrote the paper.

Supplementary material

Supplementary material is available at *Brain* online.

References

1. Saudou F, Humbert S. The Biology of Huntingtin. *Neuron*. 2016;89(5):910-926. doi:10.1016/j.neuron.2016.02.003
2. Zuccato C, Valenza M, Cattaneo E. Molecular Mechanisms and Potential Therapeutical Targets in Huntington's Disease. *Physiological Reviews*. 2009;90(3):905-981. doi:10.1152/physrev.00041.2009
3. Rüb U, Seidel K, Heinsen H, Vonsattel JP, den Dunnen WF, Korf HW. Huntington's disease (HD): the neuropathology of a multisystem neurodegenerative disorder of the human brain. *Brain Pathology*. 2016;26(6):726-740. doi:10.1111/bpa.12426

4. Valenza M, Leoni V, Tarditi A, et al. Progressive dysfunction of the cholesterol biosynthesis pathway in the R6/2 mouse model of Huntington's disease. *Neurobiology of Disease*. 2007;28(1):133-142. doi:10.1016/j.nbd.2007.07.004
5. Valenza M, Carroll JB, Leoni V, et al. Cholesterol biosynthesis pathway is disturbed in YAC128 mice and is modulated by huntingtin mutation. *Human Molecular Genetics*. 2007;16(18):2187-2198. doi:10.1093/hmg/ddm170
6. Kacher R, Lamazière A, Heck N, et al. CYP46A1 gene therapy deciphers the role of brain cholesterol metabolism in Huntington's disease. *Brain*. 2019;142(8):2432-2450. doi:10.1093/brain/awz174
7. Shankaran M, di Paolo E, Leoni V, et al. Early and brain region-specific decrease of de novo cholesterol biosynthesis in Huntington's disease: A cross-validation study in Q175 knock-in mice. *Neurobiology of Disease*. 2017;98:66-76. doi:10.1016/j.nbd.2016.11.013
8. Leoni V, Mariotti C, Tabrizi SJ, et al. Plasma 24S-hydroxycholesterol and caudate MRI in pre-manifest and early Huntington's disease. *Brain*. 2008;131(11):2851-2859. doi:10.1093/brain/awn212
9. Leoni V, Mariotti C, Nanetti L, et al. Whole body cholesterol metabolism is impaired in Huntington's disease. *Neuroscience Letters*. 2011;494(3):245-249. doi:10.1016/j.neulet.2011.03.025
10. Leoni V, Long JD, Mills JA, di Donato S, Paulsen JS. Plasma 24S-hydroxycholesterol correlation with markers of Huntington disease progression. *Neurobiology of Disease*. 2013;55:37-43. doi:10.1016/j.nbd.2013.03.013
11. Jurevics H, Morell P. Cholesterol for synthesis of myelin is made locally, not imported into brain. *Journal of Neurochemistry.* 1995;64(2),895-901. doi:10.1046/j.1471-4159.1995.64020895.x.
12. Björkhem I, Meaney S, Fogelman AM. Brain Cholesterol: Long Secret Life behind a Barrier. *Arteriosclerosis, Thrombosis, and Vascular Biology*. 2004;24(5):806-815. doi:10.1161/01.ATV.0000120374.59826.1b
13. Li D, Zhang J, Liu Q. Brain cell type-specific cholesterol metabolism and implications for learning and memory. *Trends in Neurosciences*. 2022;45(5):401-414. doi:10.1016/j.tins.2022.01.002
14. Valenza M, Chen JY, di Paolo E, et al. Cholesterol-loaded nanoparticles ameliorate synaptic and cognitive function in H untington's disease mice. *EMBO Molecular Medicine*. 2015;7(12):1547-1564. doi:10.15252/emmm.201505413

15. Birolini G, Valenza M, di Paolo E, et al. Striatal infusion of cholesterol promotes dose-dependent behavioral benefits and exerts disease-modifying effects in Huntington's disease mice. *EMBO Molecular Medicine*. 2020;12(10). doi:10.15252/emmm.202012519
16. Belletti D, Grabrucker AM, Pederzoli F, et al. Hybrid nanoparticles as a new technological approach to enhance the delivery of cholesterol into the brain. *International Journal of Pharmaceutics*. 2018;543(1-2):300-310. doi:10.1016/j.ijpharm.2018.03.061
17. Birolini G, Valenza M, Ottonelli I, et al. Insights into kinetics, release, and behavioral effects of brain-targeted hybrid nanoparticles for cholesterol delivery in Huntington's disease. *Journal of Controlled Release*. 2021;330:587-598. doi:10.1016/j.jconrel.2020.12.051
18. Southwell AL, Smith-Dijak A, Kay C, et al. An enhanced Q175 knock-in mouse model of Huntington disease with higher mutant huntingtin levels and accelerated disease phenotypes. *Human Molecular Genetics*. 2016;25(17):3654-3675. doi:10.1093/hmg/ddw212
19. Passoni A, Favagrossa M, Colombo L, Bagnati R, Gobbi M, Diomede L, Birolini G, Di Paolo E, Valenza M, Cattaneo E, Salmona M. Efficacy of Cholesterol Nose-to-Brain Delivery for Brain Targeting in Huntington's Disease. *ACS Chemical Neuroscience*. 2020;11(3):367-372. doi: 10.1021/acschemneuro.9b00581
20. Birolini G, Verlengia G, Talpo F, et al. SREBP2 gene therapy targeting striatal astrocytes ameliorates Huntington's disease phenotypes. *Brain*. 2021;144(10):3175-3190. doi:10.1093/brain/awab186/6273579
21. Valenza M, Leoni V, Karasinska JM, et al. Cholesterol defect is marked across multiple rodent models of Huntington's disease and is manifest in astrocytes. *Journal of Neuroscience*. 2010;30(32):10844-10850. doi:10.1523/JNEUROSCI.0917-10.2010
22. Cepeda C, Wu N, André VM, Cummings DM, Levine MS. The Corticostriatal Pathway in Huntington's Disease. *Progress in Neurobiology*. 2006;81(5-6):253-271. doi: 10.1016/j.pneurobio.2006.11.001
23. Milnerwood AJ, Raymond LA. Early synaptic pathophysiology in neurodegeneration: Insights from Huntington's disease. *Trends in Neurosciences*. 2010;33(11):513-523. doi:10.1016/j.tins.2010.08.002
24. Heikkinen T, Lehtimäki K, Vartiainen N, et al. Characterization of Neurophysiological and Behavioral Changes, MRI Brain Volumetry and 1H MRS in zQ175 Knock-In Mouse Model of Huntington's Disease. *PLoS ONE*. 2012;7(12). doi:10.1371/journal.pone.0050717

25. Indersmitten T, Tran CH, Cepeda C, Levine MS. Altered excitatory and inhibitory inputs to striatal medium-sized spiny neurons and cortical pyramidal neurons in the Q175 mouse model of Huntington's disease. *Journal of Neurophysiology.* 2015;113(7):2953-66. doi: 10.1152/jn.01056.2014
26. Vezzoli E, Caron I, Talpo F, et al. Inhibiting pathologically active ADAM10 rescues synaptic and cognitive decline in Huntington's disease. *Journal of Clinical Investigation*. 2019;129(6):2390-2403. doi:10.1172/JCI120616
27. Boussicault L, Alves S, Lamazière A, et al. CYP46A1, the rate-limiting enzyme for cholesterol degradation, is neuroprotective in Huntington's disease. *Brain*. 2016;139(3):953-970. doi:10.1093/brain/awv384
28. Rao AK, Gordon AM, Marder KS. Coordination of fingertip forces during precision grip in premanifest Huntington's disease. *Movement Disorders*. 2011;26(5):862-869. doi:10.1002/mds.23606
29. Paulsen JS, Nance M, Kim JI, et al. A review of quality of life after predictive testing for and earlier identification of neurodegenerative diseases. *Progress in Neurobiology*. 2013;110:2-28. doi:10.1016/j.pneurobio.2013.08.003
30. Ramos ARS, Garrett C. Huntington's Disease: Premotor Phase. *Neurodegenerative Diseases*. 2017;17(6):313-322. doi:10.1159/000481172
31. Asif-Malik A, Dautan D, Young AMJ, Gerdjikov T v. Altered cortico-striatal crosstalk underlies object recognition memory deficits in the sub-chronic phencyclidine model of schizophrenia. *Brain Structure and Function*. 2017;222(7):3179-3190. doi:10.1007/s00429-017-1393-3
32. Darvas M, Palmiter RD. Restriction of Dopamine Signaling to the Dorsolateral Striatum Is Sufficient for Many Cognitive Behaviors Dopaminergic Signaling Is Necessary for Object Memory, Visuospatial, and Discriminatory Learning. Without Any Treatment, DD Mice Did Not Explore Any of the Objects in an Object Recognition Task. Stimulation of DD Mice with Caffeine Restored Object Explora. *The Proceedings of the National Academy of Sciences.* 2009;106(34):14664-14669. doi:10.1073/pnas.0907299106
33. Poulter SL, Kosaki Y, Sanderson DJ, McGregor A. Spontaneous object-location memory based on environmental geometry is impaired by both hippocampal and dorsolateral striatal lesions. *Brain and Neuroscience Advances*. 2020;4:239821282097259. doi:10.1177/2398212820972599

34. Krabbe S, Gründemann J, Lüthi A. Amygdala Inhibitory Circuits Regulate Associative Fear Conditioning. *Biological Psychiatry*. 2018;83(10):800-809. doi: 10.1016/j.biopsych.2017.10.006
35. Goodroe SC, Starnes J, Brown TI. The Complex Nature of Hippocampal-Striatal Interactions in Spatial Navigation. *Frontiers in Human Neuroscience*. 2018;12. doi:10.3389/fnhum.2018.00250
36. Calabresi P, Pisani A, Mercuri NB, Bernardi G. On the mechanisms underlying hypoxia-induced membrane depolarization in striatal neurons. *Brain* 1995;118(4):1027-1038. doi: 10.1093/brain/118.4.1027
37. Klapstein GJ, Fisher RS, Zanjani H, et al. Electrophysiological and Morphological Changes in Striatal Spiny Neurons in R6/2 Huntington's Disease Transgenic Mice. *Journal of Neurophysiology*. 2001;86(6):2667-2677. doi: 10.1152/jn.2001.86.6.2667
38. Ramot Y, Ben-Eliahu S, Kagan L, Ezov N, Nyska A. Subcutaneous and Intraperitoneal Lipogranulomas Following Subcutaneous Injection of Olive Oil in Sprague-Dawley Rats. *Toxicologic Pathology*. 2009;37(7):882-886. doi:10.1177/0192623309347911
39. Alsina-Sanchis E, Mülfarth R, Moll I, Mogler C, Rodriguez-Vita J, Fischer A. Intraperitoneal oil application causes local inflammation with depletion of resident peritoneal macrophages. *Molecular Cancer Research*. 2021;19(2):288-300. doi:10.1158/1541-7786.MCR-20-0650

Figure legends

Figure 1. Cognitive and motor abilities of zQ175DN mice following 1 cycle of g7-hybrid-NPs-chol at pre-symptomatic stage ("early cohort") and at symptomatic stage ("late cohort"). (**A**) Experimental paradigm of the "early cohort": zQ175DN mice (n=9-18) were treated with g7-hybrid-NPs-chol (0.12 mg NPs/gr body weight) from 5 to 9 weeks of age with 2 ip injection/week. Wt (n=10-13) and zQ175DN (n=10-11) littermates were treated with saline solution as controls. Novel Object Recognition (NOR), Paw Clasping (PC), Grip Strength (GS), and Activity Cage (AC) tests were performed at 20-29-35-45 weeks of age, Rotarod (RR) at 46 weeks of age, Fear Conditioning (FC) at 48 weeks of age. Mice were sacrificed at 50 weeks of age. (**B**) Discrimination index (DI; %) above zero indicates a preference for the novel object; DI below zero indicates a preference for the familiar object. (**C**) Paw Clasping score.

(**D**) Grip Strength (grams). (**E**) Latency to fall (seconds) from an accelerating Rotarod. (**F**) Experimental paradigm of the "late cohort": zQ175DN mice (n=13-14) were treated with g7-hybrid-NPs-chol (0.12 mg NPs/gr body weight) from 21 weeks of age to 25 weeks of age with 2 ip injection/week. Wt (n=13-14) and zQ175DN (n=13-14) littermates were treated with saline solution as controls. NOR, PC, GS, and AC were performed at 40-49 weeks of age, RR at 50 weeks of age, FC at 51 weeks of age, and mice were sacrificed at 51 weeks of age. (**G**) Discrimination index (DI; %) in the NOR test. (**H**) Paw Clasping score (**I**) Grip Strength (grams); (**J**) Latency to fall (seconds) from an accelerating Rotarod.

The data in B-E are from three independent trials and shown as scatterplot graphs with mean±SEM. The data in G–J are from two independent trials and shown as scatterplot graphs with mean±SEM. Each dot (B, D–G, I, J–N) corresponds to the value obtained from each animal. Statistics: one-way ANOVA with Tuckey post-hoc test (*p<0.05; **p<0.01; ***p<0.001; ****p<0.0001).

Figure 2. Cognitive and motor abilities of zQ175DN mice following 2 cycles of g7-hybrid-NPs-chol ("2 cycles cohort"). (**A**) Experimental paradigm of the "2 cycles cohort": zQ175DN mice (n=9-17) were treated with g7-hybrid-NPs-chol (0.12 mg NPs/gr body weight) from 5 weeks of age to 9 weeks of age with 2 ip injection/week. The treatment was repeated from 21 to 25 weeks of age. Wt (n=15-21) and zQ175DN (n=11-21) littermates were treated with saline solution as controls. Novel Object Recognition (NOR), Paw Clasping (PC), Grip Strength (GS), and Activity Cage (AC) were performed at 20-29-35-45 weeks of age, Y-maze (YM) test at 30-48 weeks of age, Rotarod (RR) at 46 weeks of age, Fear Conditioning (FC) at 48 weeks of age. Mice were sacrificed at 51 weeks of age. (**B**) Discrimination index (DI; %) in the NOR test. (**C**) Number of freezing episodes measured during the Fear Conditioning (cued paradigm). (**D**) Paw Clasping score. (**E**) Grip Strength (grams). (**F**) Latency to fall (seconds) from an accelerating Rotarod. (**G-H**) Global motor activity (G) and total distance traveled (H) in an Activity Cage test. The data in B–H are from three independent trials and shown as scatterplot graphs with mean±SEM. Each dot (B, D–H) corresponds to the value obtained from each animal. Statistics: one-way ANOVA with Tuckey post-hoc test (*p<0.05; **p<0.01; ***p<0.001; ****p<0.0001).

Figure 3. Segregation of the behavioral tasks in cholesterol treated HD mice with wt versus HD mice

(**A**) Heat maps summarizing the behavior related to NOR, Paw Clasping, Grip Strength and Activity Cage tests of all cohorts using conditional formatting (excel). Green (+): good performance; red (-): bad performance. (**B, C**) Principal component analysis by combining all the values related to motor and cognitive tasks from all mice at 29 weeks (B) and 45-49 weeks of age (C). The ellipses were calculated with a 95% confidence interval around the centroid of each group. (**D**) Graphical representation and statistical analysis of the overall cognitive performance assessed by NOR test among wt, HD and HD cholesterol-treated mice, comprehensive of data collected from five different studies. Differences between wt, HD, and HD+chol groups have been assessed using one way Welch's ANOVA followed by pairwise Welch's t-test with Bonferroni correction performed with R package rstatix vv 0.7.0.

Figure 4. Sterols in the striatum of zQ175DN mice following cholesterol treatment in the "early cohort", "late cohort" and "2 cycles cohort". (A-B) Cholesterol (A) and lathosterol (B) content quantified by mass spectrometry in the striatum of animals (n=4/group) from the "early cohort" (at 29 and 50week), "late cohort" (at 51week) and "2 cycles cohort" (at 50week). The data in A-B are shown as scatterplot graphs with mean±SEM. Each dot corresponds to the value obtained from each animal. Statistics: one-way ANOVA with Tuckey post-hoc test (*p<0.05; **p<0.01; ***p<0.001; ****p<0.0001).

Figure 5. Mutant HTT aggregates in the striatum and cortex of zQ175DN mice following cholesterol treatment in the "early cohort", "late cohort" and "2 cycles cohort". (**A**–**G**) Experimental scheme and immunolabeling of muHTT aggregates in brain coronal slices of zQ175DN and zQ175DN+chol mice from "early cohort" at 29 and 50 weeks of age (n=3/group). Zoom of representative confocal images of immunostaining against muHTT aggregates (green) showing muHTT aggregates positive for EM48 antibody in the striatum (B) and cortex (E) and relative quantification of number and size of aggregates (C-G). (**H-N**) Experimental scheme and immunolabeling of muHTT aggregates in brain coronal slices of zQ175DN and zQ175DN+chol mice from "late cohort" at 51 weeks of age (n=3/group). Zoom of representative confocal images of immunostaining against muHTT aggregates (green) showing muHTT aggregates positive for EM48 antibody in the striatum (I) and cortex (L) and

relative quantification of number and size of aggregates (J-K and M-N). (**O-U**) Experimental scheme and immunolabeling of muHTT aggregates in brain coronal slices of zQ175DN and zQ175DN+chol mice from "2 cycles cohort" at 50 weeks of age (n=3/group). Zoom of representative confocal images of immunostaining against muHTT aggregates (green) showing muHTT aggregates positive for EM48 antibody in the striatum (P) and cortex (S) and relative quantification of number and size of aggregates (Q-R and T-U).

Hoechst (Ho, blue) was used to counterstain nuclei. Scale bar: 20 µm. 10 images/animal were analyzed from 9 sections throughout the entire striatum and cortex. The data in C-D, F-G, J-K, <m-N, Q-R, T-U are shown as scatterplot graphs with mean±SEM. Each dot corresponds to the value obtained from each image. Statistics: Student's t-test (**p<0.01; ***p<0.001; ****p<0.0001).

Figure 6. Electrophysiological analysis in MSNs of zQ175DN mice following cholesterol treatment in the "2 cycles cohort". (**A**–**C**) Membrane Capacitance (Cm, A), Resting Potential (mV; B) and Input Resistance (Rin, C) recorded from MSNs of wt (6 cells from 3 mice), zQ175DN (8 cells from 4 mice) and zQ175DN+chol mice (5 cells from 3 mice) from "2 cycles cohort". (**D**) Representative traces of spontaneous EPSCs (sEPSCs) at a holding potential of -70 mV. (**E**–**F**) Inter-event intervals (inverse of the frequency) of spontaneous (sEPSCs) (E) and miniature EPSCs (mEPSCs) (F) recorded from MSNs of wt, zQ175DN and zQ175DN+chol mice. (**G**–**H**) Cumulative inter-event histogram showing the release probability of sEPSCs (G) and mEPSCs (H) in all three groups. (**I–J**) Correlation matrix showing the Spearman correlation between behavioral tasks and sEPSC and mEPSC (I) and bubble dot plot chart representing the p-values of the correlation in I (J).

The data in A, B, C, E, and F are shown as scatterplot graphs with means±standard error. Each dot corresponds to the value obtained from each cell. Statistics (A-B-C-E-F): one-way ANOVA with Tuckey post-hoc test (*p<0.05; **p<0.01). Statistics (G-H): one-way ANOVA with Bonferroni post-hoc test (*p<0.05; **p<0.005; ***P<0,001).

Figure 1

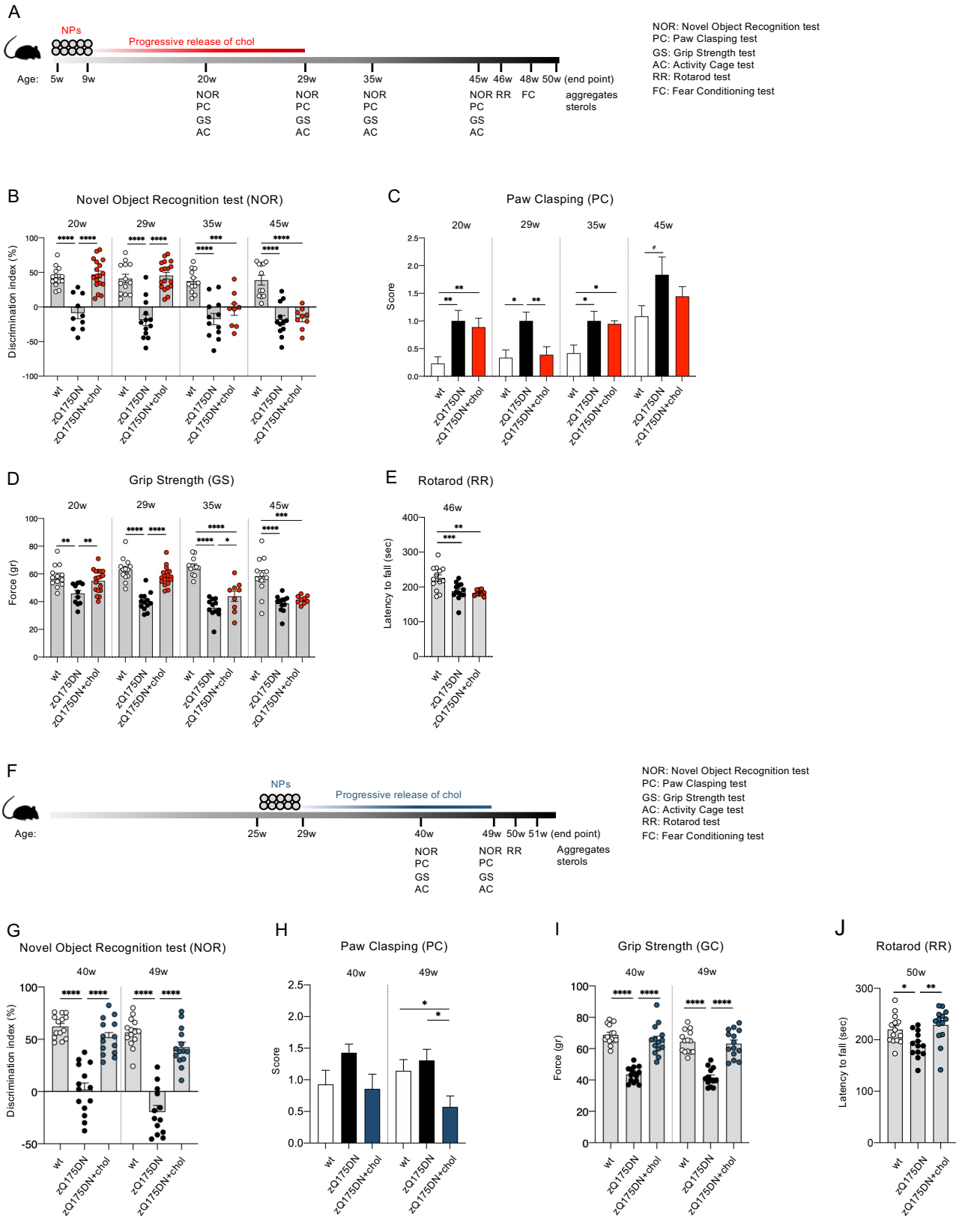

Figure 2

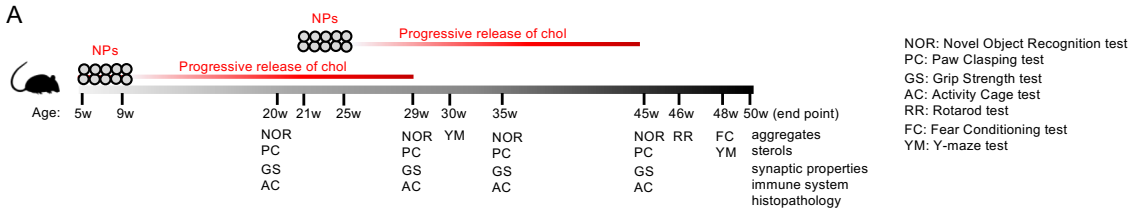

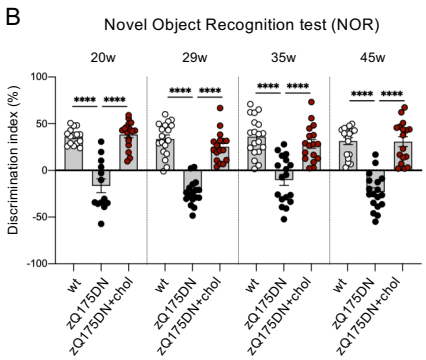

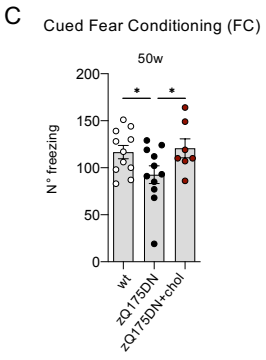

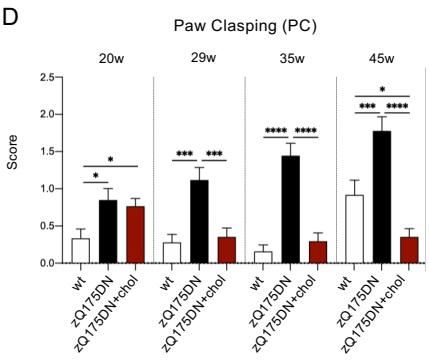

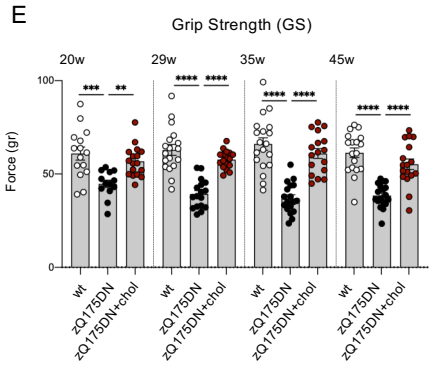

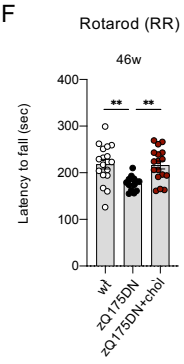

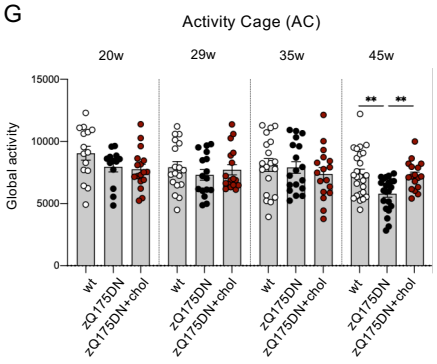

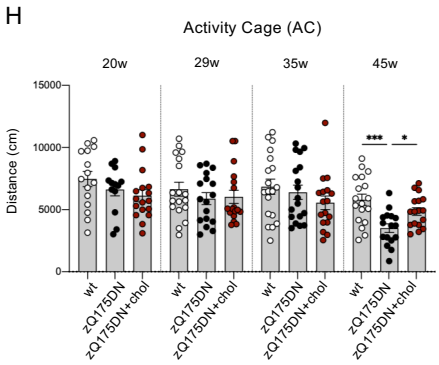

Figure 3

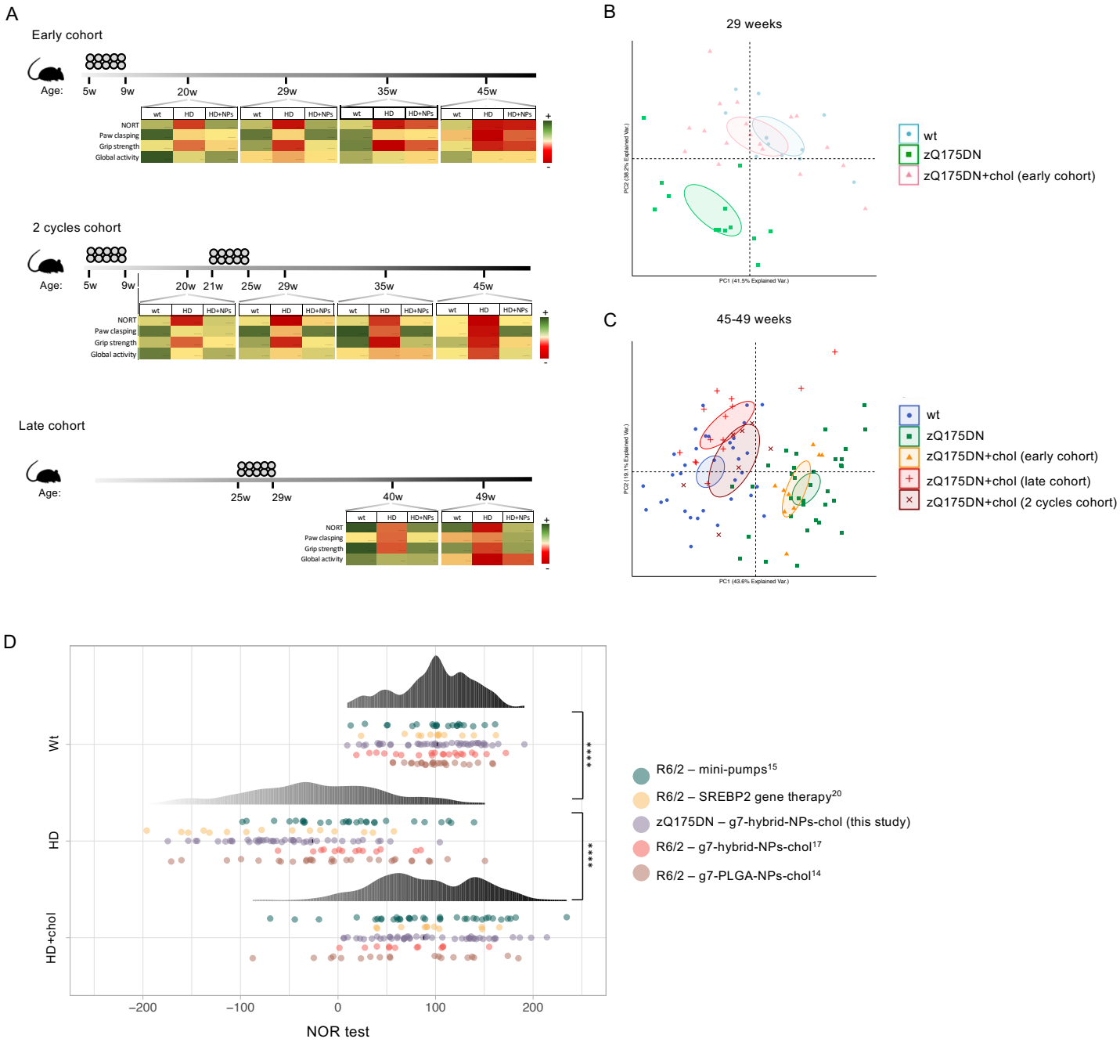

Figure 4

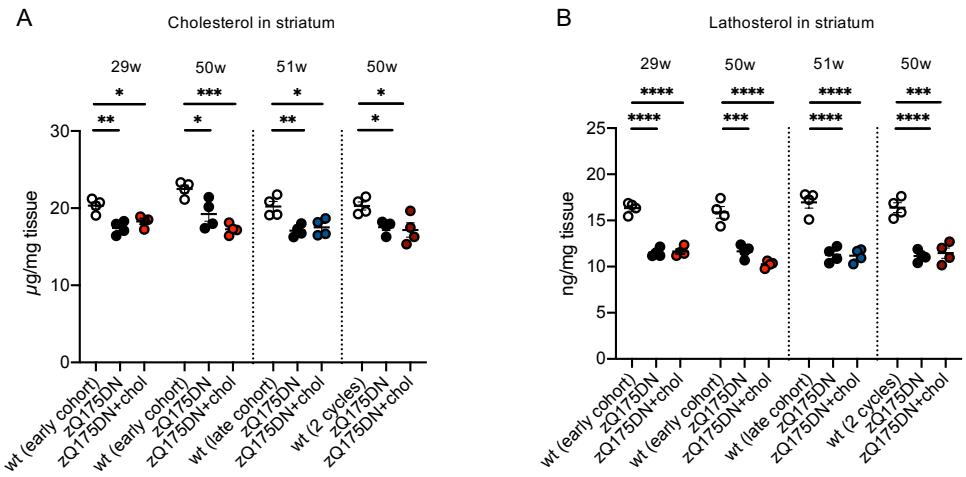

Figure 5

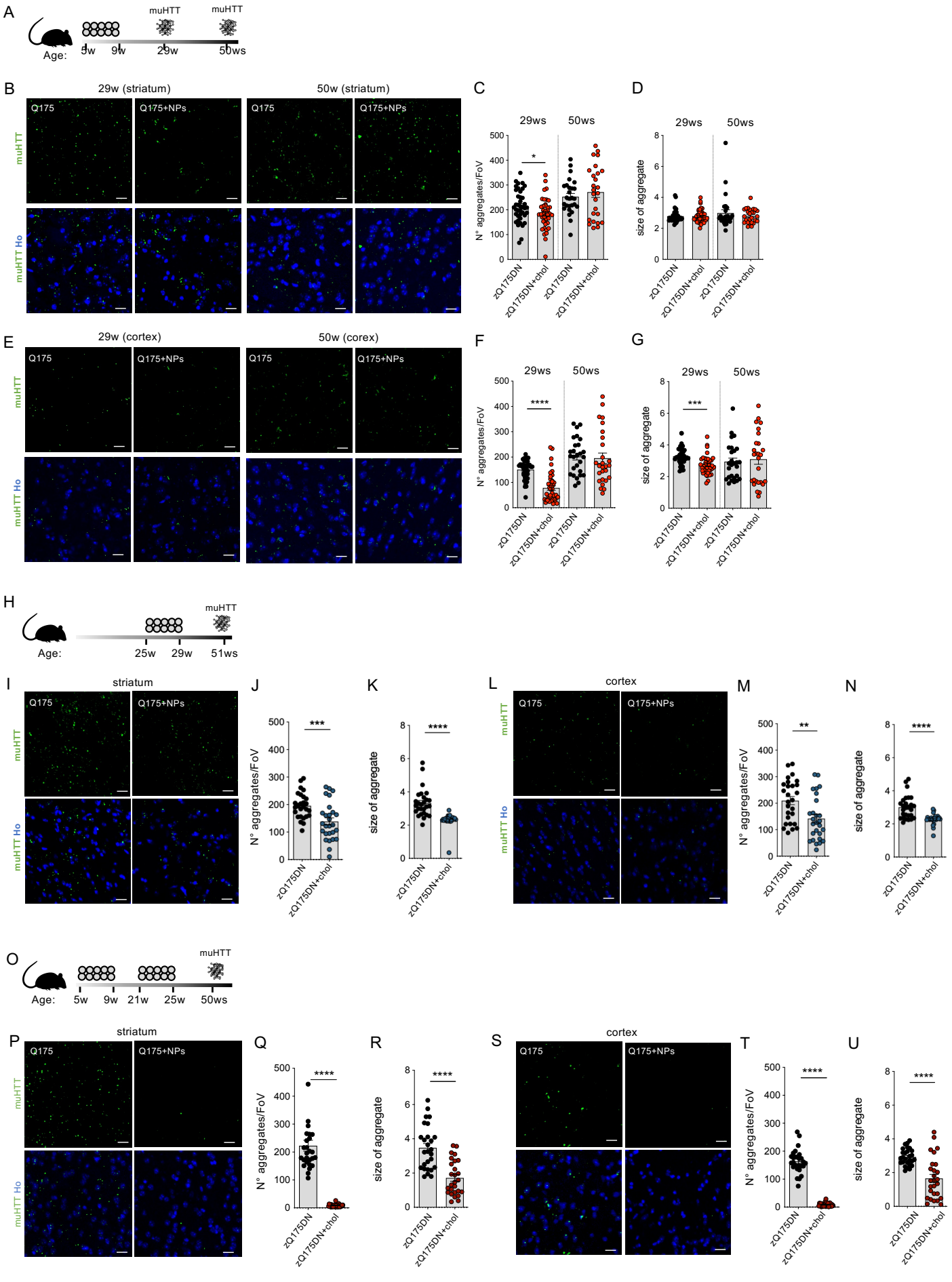

Figure 6